Available online at www.sciencedirect.com
SCIENCE DIRECT®
Journal of Solid State Chemistry 179 (2006) 464–469
JOURNAL OF SOLID STATE CHEMISTRY
www.elsevier.com/locate/jssc

Two new titanium molybdenum arsenides: Ti_2MoAs_2 and Ti_3MoAs_3, ternary substitution variants of V_3As_2 and β-V_4As_3

Abdeljalil Assoud, Shahab Derakhshan, Katja M. Kleinke, Holger Kleinke*

Department of Chemistry, University of Waterloo, Waterloo, Ont., Canada N2L 3G1

Received 19 September 2005; received in revised form 31 October 2005; accepted 7 November 2005
Available online 7 December 2005

Abstract

The title compounds were prepared by arc-melting pre-annealed mixtures of Ti, Mo, and As. Both Ti_2MoAs_2 and Ti_3MoAs_3 adopt structures formed by the corresponding binary vanadium arsenides, V_3As_2 and β-V_4As_3. Ti_2MoAs_2 crystallizes in the tetragonal space group $P4/m$, with $a = 9.706(4)$ Å, $c = 3.451(2)$ Å, $V = 325.1(3)$ Å^3 ($Z = 4$), and Ti_3MoAs_3 in the monoclinic space group $C2/m$, with $a = 14.107(3)$ Å, $b = 3.5148(7)$ Å, $c = 9.522(2)$ Å, $\beta = 100.66(3)^\circ$, $V = 464.0(2)$ Å^3 ($Z = 4$). In both cases, the metal atoms form infinite chains of trans edge-condensed octahedra, and the As atoms are located in (capped) trigonal prismatic voids. While most metal atom sites exhibit mixed Ti/Mo occupancies, the Mo atoms prefer the sites with more metal atom and fewer As atom neighbors. Ti_2MoAs_2 and Ti_3MoAs_3 are metallic entropy-stabilized materials that decompose upon annealing at intermediate temperatures.

Keywords: Crystal structure; Electronic structure; Mixed occupancies; Arsenide

1. Introduction

The concept of obtaining new materials, often with new structure types, by using two different yet similar transition metals was described as DFSO model (DFSO: differential fractional site occupancies) [1,2]. The discovery of four ternary niobium tantalum sulfides with mixed Nb/Ta occupancies, whose structures were not known in either of the binary systems (Nb/S; Ta/S) [3–6], led to the formulation of this model. Several ternary valence-electron poor transition metal antimonides exhibiting mixed occupancies on the metal atom sites were discovered in recent years. Examples include mixed occupancies of Ti and Zr (in (Zr,Ti)Sb [7] and $(Zr,Ti)_5Sb_8$ [8]), Ti and Hf ($(Hf,Ti)_5Sb_8$ [8] and $(Hf,Ti)_7Sb_4$ [9]), Zr and V ($(Zr,V)_{13}Sb_{10}$ [10] and $(Zr,V)_{11}Sb_8$ [11]).

Very few compounds are known to exist with mixed occupancies of elements of groups 4 and 6. These include phosphides ($(Hf,Mo)_2P$ [12]), arsenides ($(Ti,Mo)_5As_3$ [13]) and antimonides ($(Ti,Mo)_8Sb_9$ [14]). The two Ti/Mo materials exist only with high Ti:Mo ratios between 4:1 and 2:1. As they form structures adopted by V-deficient pnictides, namely $V_{4.95}As_3$ [15] and $V_{7.5}Sb_9$ [16], respectively, we hypothesized that Ti/Mo compounds generally may imitate V compounds. Subsequently we discovered Ti_2MoAs_2 and Ti_3MoAs_3, the ternary substitution variants of V_3As_2 [17] and β-V_4As_3 [18].

2. Experimental

2.1. Synthesis and analysis

The elements were used as acquired from ALFA AESAR (Ti: powder −150 mesh, 99.9% purity; Mo: powder 3–7 μm, 99.9%) and ALDRICH (As: powder, 99.5%). In the first step, the elements were pre-heated in evacuated silica tubes at 700 °C over a period of 5 days. An As excess was added to compensate for the weight loss during subsequent arc-melting caused by the vapor pressure of As. The mixtures (each of 400–500 mg) were thoroughly ground, and then pressed into a round pellet of

*Corresponding author. Fax: +519 746 0435.
E-mail address: kleinke@uwaterloo.ca (H. Kleinke).

0022-4596/$ - see front matter © 2005 Elsevier Inc. All rights reserved.
doi:10.1016/j.jssc.2005.11.007

6 mm diameter. In the final step, the pellets were arc-melted once, and again after inversion on a water-cooled copper block under a flow of argon. The *M*: As starting ratios were 3:2.25 for M_3As_2, and 4:3.2 for M_4As_3 ($M = Ti + Mo$), corresponding to excesses of As of 12.5% and 6.7%, respectively. The Ti:Mo ratios were varied in small increments of 0.5; and only the 2:1 starting ratio for M_3As_2, and the 3:1 ratio for M_4As_3 resulted in pure products, indicating negligible phase widths in both cases. Annealing of the products over a period of 5 days both at 900 and 1200 °C resulted in decomposition into known binary arsenides and elemental molybdenum. Starting from a 5:3 ratio of Ti:Mo the α-modification of V_4As_3 [19] formed presumably, as became evident from a single crystal study [20].

In all cases, phase identification was performed via X-ray powder diffraction utilizing Cu $K\alpha_1$ radiation with an INEL powder diffractometer equipped with position-sensitive detector. Energy dispersive analysis of X-rays (EDX) investigations using an electron microscope (LEO 1530) with an additional EDX device (EDAX Pegasus 1200) were performed on selected crystals out of the two homogenous reaction mixtures. The scans were performed with an acceleration voltage of 21 kV under high dynamic vacuum. No impurity elements (e.g., Si, O, or Cu, stemming from the reaction container) were detected.

2.2. Crystal structure studies

Single crystals were selected with the aid of an optical microscope for the structure studies, performed on the Smart APEX CCD (BRUKER, utilizing Mo-*K*α radiation). In the case of the monoclinic Ti_3MoAs_3, the scans were done each over 0.3° in ω in two groups of 606 frames (each with an exposure time of 60 s) at $\phi = 0°$ and 60°. For the smaller, tetragonal crystal of Ti_2MoAs_2, one group of scans of 0.25° at $\phi = 0°$ was chosen, with an exposure time of 120 s per frame.

The data were corrected for Lorentz and polarization effects. Absorption corrections were based on fitting a function to the empirical transmission surface as sampled by multiple equivalent measurements using SADABS [21]. The structure refinements (SHELXL package [22]) were commenced with the atomic positions taken from V_3As_2 and β-V_4As_3, respectively, as listed in the ICSD database. Initially all V positions were assigned to be mixed occupied by Ti and Mo without deficiencies. Only in case of the *M*3 site of Ti_2MoAs_2, the occupancy was refined to be 100% Ti within its standard deviation σ, while all the other sites exhibited mixtures ranging from 3.8(9)% Mo to 98.0(7)% Mo, including intermediate values such as 34.2(4)% Mo. Some of these refined values are at the borderline of significance, i.e. within four σ; for the sake of clarity we include all values larger than 2σ. An extinction correction was not required for Ti_2MoAs_2, and the extinction parameter for Ti_3MoAs_3 was refined to be just above its standard deviation. The refined stoichiometries were $Ti_{2.02(1)}Mo_{0.98}As_2$ and $Ti_{3.03(4)}Mo_{0.97}As_3$, i.e. within 2σ of the idealized formulas Ti_2MoAs_2 and Ti_3MoAs_3. Details of the structure determination are given in Table 1, and atomic positions with equivalent displacement parameters may be found in Tables 2 and 3. Further details of the crystal structure investigations can be obtained from the Fachinformationszentrum Karlsruhe, 76344 Eggenstein-Leopoldshafen, Germany, on quoting the depository numbers CSD-415708 and CSD-415709.

2.3. Electronic structure calculations

Four band structures were calculated employing the self-consistent tight-binding *first principles* linear muffin tin orbitals (LMTO) approximations [23,24]. In the LMTO approach, the density functional theory is used with the local density approximation (LDA) [25]. Integrations in *k* space were performed by an improved tetrahedron method [26] on sufficient *k* points of the first Brillouin zone. Integrated COHP values (ICOHPs) of selected bonds were extracted from the energy-partitioning Crystal Orbital Hamilton Population scheme [27] to gain information about the bond strengths, comparable to the longer established Mulliken Overlap Populations [28] extracted from the Crystal Orbital Overlap Populations [29]. The chosen models were based on the reported V_3As_2 and β-V_4As_3 structures, as well as our refined models of Ti_2MoAs_2 and Ti_3MoAs_3. In case of Ti_2MoAs_2, *M*2 (refined as 16.9(4)% Mo and 83.1% Ti) and *M*3 (refined as Ti) were treated as Ti sites, and *M*4 (98.0(7)% Mo) and *M*5 (89.7(7)% Mo) as Mo sites. Two of the four *M*1 sites per cell were simulated as Mo and two as Ti, for the refined Mo occupancy was 34.2(4)%. This led to a symmetry reduction from *P*4/*m* to *P*2/*m*, and the anticipated formula of Ti_2MoAs_2. In case of Ti_3MoAs_3, Ti was assigned to the sites *M*1–*M*3 (refined Mo occupancies below 15%), and Mo to *M*5 (refined to 95.9(1)% Mo). Last, *M*4 (refined to 24.6(9)% Mo) was half occupied by Mo in our model, i.e. two of the four sites per cell. This necessitated a symmetry reduction from *C*2/*m* to *Cm*, yielding the correct formula Ti_3MoAs_3.

3. Results and discussion

3.1. Crystal structures

The structure types of Ti_2MoAs_2 and Ti_3MoAs_3 are V_3As_2 [17] and Cr_4As_3 [30], respectively. V_4As_3 exists in two modifications, α and β: β-V_4As_3—the high temperature form—is isotypic with Cr_4As_3 [18]. As these structure types were discussed before, the description will be kept short here. V_3As_2 can be understood as a V-inserted Ti_5Te_4 [31] structure ($V_3As_2 \equiv V_5As_4V$), thereby comprising linear chains of face-sharing centered V cubes, as in body-centered cubic (bcc) elemental vanadium, surrounded by As atoms, with the additional V atom located in octahedral voids of the As atom substructure. The latter is called *M*3

Table 1
Crystallographic data for Ti_2MoAs_2 and Ti_3MoAs_3

Empirical formula	$Ti_{2.02(1)}Mo_{0.98}As_2$	$Ti_{3.03(4)}Mo_{0.97}As_3$
Formula weight	340.38 g/mol	925.92 g/mol
Temperature	298(2) K	298(2) K
Wavelength	0.71073 Å	0.71073 Å
Crystal system	Tetragonal	Monoclinic
Space group	$P4/m$	$C2/m$
Unit cell dimensions	$a = 9.706(4)$ Å $c = 3.451(2)$ Å $V = 325.1(3)$ Å^3	$a = 14.107(3)$ Å $b = 3.5148(7)$ Å $c = 9.522(2)$ Å $\beta = 100.66(3)^\circ$ $V = 464.0(2)$ Å^3
Z	4	4
Density (calculated)	6.954 g/cm^3	6.628 g/cm^3
Absorption coefficient	28.459 mm^{-1}	28.628 mm^{-1}
$F(000)$	606	826
Crystal size	$0.04 \times 0.04 \times 0.02$ mm	$0.06 \times 0.04 \times 0.03$ mm
Reflections collected	1342	1938
Independent reflections	547 [R(int) = 0.0515]	772 [R(int) = 0.0346]
Completeness to $\theta = 30^\circ$	99.6%	99.7%
Refinement method	Full-matrix least-squares on F^2	Full-matrix least-squares on F^2
Data\restraints\parameters	547\0\37	772\0\51
R indices (all data)	$R1 = 0.0428$, w$R2 = 0.0718$	$R1 = 0.0417$, w$R2 = 0.0850$
Extinction coefficient	0	0.0004(3)
Largest diff. peak and hole	1.92 and -1.39 e$^-$/Å^3	2.08 and -1.33 e$^-$/Å^3

Table 2
Atomic positions and equivalent temperature factors of Ti_2MoAs_2

Atom	Site	x	y	z	U_{eq}/Å^2	Occ.
$M1$	4k	0.1382(1)	0.1764(1)	$\frac{1}{2}$	0.0085(4)	0.342(4) Mo, 0.658 Ti
$M2$	4j	0.3975(1)	0.2826(1)	0	0.0070(4)	0.169(4) Mo, 0.831 Ti
$M3$	2f	0	$\frac{1}{2}$	$\frac{1}{2}$	0.0115(5)	1 Ti
$M4$	1d	$\frac{1}{2}$	$\frac{1}{2}$	$\frac{1}{2}$	0.0061(4)	0.980(7) Mo, 0.020 Ti
$M5$	1a	0	0	0	0.0071(5)	0.897(7) Mo, 0.103 Ti
As1	4k	0.24703(8)	0.41141(9)	$\frac{1}{2}$	0.0069(2)	1
As2	4j	0.28706(9)	0.03457(8)	0	0.0084(2)	1

Table 3
Atomic positions and equivalent temperature factors of Ti_3MoAs_3

Atom	Site	x	y	z	U_{eq}/Å^2	Occ.
$M1$	2a	0	0	0	0.0075(7)	0.15(1) Mo, 0.85 Ti
$M2$	4i	0.6577(1)	0	0.4470(1)	0.0072(5)	0.134(9) Mo 0.866 Ti
$M3$	4i	0.2263(1)	0	0.1747(2)	0.0090(6)	0.038(9) Mo, 0.962 Ti
$M4$	4i	0.43855(9)	0	0.2731(1)	0.0065(4)	0.246(9) Mo, 0.754 Ti
$M5$	2c	0	0	$\frac{1}{2}$	0.0060(4)	0.96(1) Mo, 0.04 Ti
As1	4i	0.07079(7)	0	0.26704(9)	0.0070(2)	1
As2	4i	0.36094(7)	0	0.00952(9)	0.0078(2)	1
As3	4i	0.82016(7)	0	0.34780(9)	0.0069(2)	1

in Ti_2MoAs_2 (left part of Fig. 1). Alternatively the metal clusters may be viewed as a chain of vertex-condensed octahedra. The *bcc* motifs (or chains of octahedra) occur in Ti_3MoAs_3 as well, where the chains run parallel to the *b*-axis. Between the chains are twice as many MAs_6 octahedra comprising $M1$ and $M3$ (right part of Fig. 1). Jeitschko et al. discussed these building blocks for a series of manganese arsenides [32].

The M atoms forming the cubes participate in fewer M–As bonds, i.e. 4–5 per M atom, compared to six for the M atoms between the cubes. The shortest bonds in these structures are between M atoms and As atoms, varying

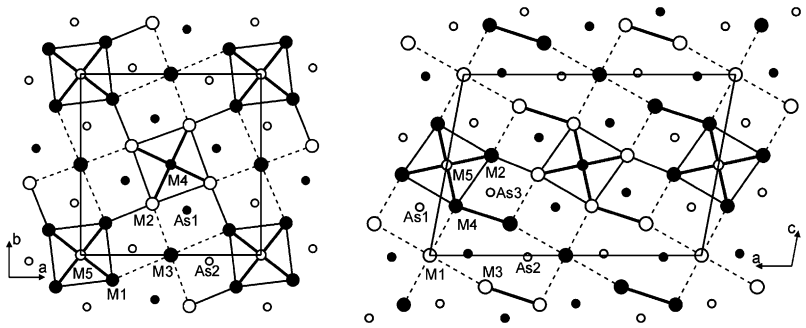

Fig. 1. Crystal structures of Ti_2MoAs_2 (left) and Ti_3MoAs_3 (right). Large circles: *M* sites; small: As. White circles are at height 0, black at $\frac{1}{2}$.

Table 4
Interatomic distances [Å] of Ti_2MoAs_2 (<3.45 Å)

*M*1–As1	1 ×	2.514(2)	*M*2–As1	2 ×	2.557(1)
*M*1–As2	2 ×	2.635(1)	*M*2–As1	2 ×	2.584(1)
*M*1–As2	2 ×	2.638(1)	*M*2–As2	1 ×	2.635(2)
*M*1–*M*5	2 ×	2.776(1)	*M*2–*M*4	2 ×	2.902(1)
*M*1–*M*1	2 ×	3.076(2)	*M*2–*M*1	2 ×	3.221(2)
*M*1–*M*2	2 ×	3.221(2)	*M*2–*M*2	2 ×	3.299(2)
*M*1–*M*3	1 ×	3.415(2)	*M*2–*M*3	2 ×	3.390(2)
*M*3–As1	2 ×	2.547(1)	*M*4–As1	4 ×	2.602(1)
*M*3–As2	4 ×	2.713(1)	*M*4–*M*2	8 ×	2.902(1)
*M*3–*M*2	4 ×	3.390(2)			
*M*3–*M*1	2 ×	3.415(2)	*M*5—As2	4 ×	2.806(1)
			*M*5—*M*1	8 ×	2.776(1)

Table 5
Interatomic distances [Å] of Ti_3MoAs_3 (<3.45 Å)

*M*1–As1	2 ×	2.554(1)	*M*2–As1	2 ×	2.598(1)
*M*1–As2	4 ×	2.6477(8)	*M*2–As3	2 ×	2.603(1)
*M*1–*M*3	2 ×	3.316(2)	*M*2–As3	1 ×	2.635(2)
*M*1–*M*4	4 ×	3.382(1)	*M*2–*M*5	2 ×	2.951(1)
			*M*2–*M*2	2 ×	3.148(2)
*M*3–As1	1 ×	2.510(2)	*M*2–*M*4	1 ×	3.208(2)
*M*3–As3	2 ×	2.598(1)	*M*2–*M*4	1 ×	3.226(2)
*M*3–As2	2 ×	2.623(1)	*M*2–*M*3	1 ×	3.417(2)
*M*3–As2	1 ×	2.681(2)			
*M*3–*M*4	1 ×	2.967(2)	*M*4–As2	1 ×	2.545(2)
*M*3–*M*2	2 ×	3.417(2)	*M*4–As1	2 ×	2.571(1)
*M*3–*M*3	1 ×	3.316(2)	*M*4–As3	2 ×	2.612(1)
			*M*4–*M*5	2 ×	2.796(1)
*M*5–As1	2 ×	2.596(1)	*M*4–*M*3	1 ×	2.967(2)
*M*5–As3	2 ×	2.679(1)	*M*4–*M*2	1 ×	3.208(2)
*M*5–*M*4	4 ×	2.796(1)	*M*4–*M*2	1 ×	3.226(2)
*M*5–*M*2	4 ×	2.951(1)			

from 2.51 to 2.81 Å in Ti_2MoAs_2 (Table 4) and 2.55–2.68 Å in Ti_3MoAs_3 (Table 5). These values compare well with the Ti–As bonds of 2.61 Å in TiAs and the Mo–As bonds of 2.52–2.75 Å in MoAs (both with six As neighbors per *M* atom).

The shortest *M*–*M* bonds occur between the center of the cubes and their corners, ranging from 2.78 to 2.90 Å in Ti_2MoAs_2 and from 2.80 to 2.95 Å in Ti_3MoAs_3. The *M*–*M* contacts along the edges of the cubes are between 3.08 and 3.30 Å in Ti_2MoAs_2 and 3.21 and 3.23 Å in Ti_3MoAs_3. Additional *M*–*M* contacts of similar lengths exist between the chains, namely 3.22 Å in Ti_2MoAs_2 and 3.15 Å in Ti_3MoAs_3. The *M*3 atom of Ti_2MoAs_2, located between the cubes, forms no short *M*–*M* bond, its shortest *M*–*M* contact being 3.39 Å. The same is true for the *M*1 atom of Ti_3MoAs_3 with the shortest *M*1–*M* distance being 3.32 Å, while the *M*3 atom is bonded to the cube via an *M*3–*M*4 bond of 2.97 Å. For comparison, a number of *M*–*M* bonds between 2.76 and 2.98 Å were found in Ti_4MoAs_3 [13].

3.2. Site preferences

There are five different M sites both in Ti_2MoAs_2 and in Ti_3MoAs_3. These may be divided into three different groups. Group 1 is formed by the M atoms of the cube centers, group 2 comprises the M atoms of the edges, and group 3 contains the interstitial M atoms between the cube chains. The sites of group 1 ($M4$, $M5$ in Ti_2MoAs_2, and $M5$ in Ti_3MoAs_3) are predominated by Mo atoms, with Ti occupancies between 2% and 10%. These positions have the fewest As neighbors (four per M atom), and the most M neighbors (eight), the latter with the shortest M–M distances. Group 2 ($M1$, $M2$ in Ti_2MoAs_2, and $M2$, $M4$ in Ti_3MoAs_3) is mixed, exhibiting Ti occupancies between 66% and 83%. Last, group 3 ($M3$ in Ti_2MoAs_2, and $M1$, $M3$ in Ti_3MoAs_3) contains mostly Ti, with Ti occupancies between 85% and 100%. This group's members participate in the longest M–M contacts, and have the highest As coordination numbers (6). Qualitatively these differences may be understood based on the smaller electronegativity of Ti, compared to Mo, leading to titanium's preference for As coordination, and the larger electron concentration of Mo, compared to Ti, resulting in more M–M bonds per Mo atom. The same trends were observed in Ti_4MoAs_3. It is noted that there are virtually no size differences between Ti and Mo, as the Pauling single bond radius of Ti is slightly larger (r_{Ti}: 1.32 Å; r_{Mo}: 1.29 Å), and Slater's crystal radius of Ti is smaller, compared to Mo (r_{Ti}: 1.40 Å; r_{Mo}: 1.45 Å) [33,34].

3.3. Electronic structure

The electronic structure of V_3As_2 was computed earlier by Bouayed et al. utilizing the Extended Hückel approximation [35]. The resulting densities of states (DOS) showed a high number of states directly at the Fermi level, E_F, albeit in a local minimum, almost exclusively of vanadium character. The latter is true for our LMTO calculations on both V_3As_2 and β-V_4As_3 (Fig. 2), where local minima appear just below the Fermi level. Metallic character is thus most likely for both arsenides, as expected for such metal-rich pnictides with a multitude of metal–metal bonds.

The energy window shown, which excludes the filled *4s* states of As, begins at −7 eV with As-*p* based states, which in part contribute to V–As bonding. The covalent character of the V–As bonds is reflected in the V contributions to the DOS at these low energies. Starting around −2 eV, the As contributions disappear, and the V-*d* states clearly dominate the area above −2 eV. Correspondingly, the bonding V–As states gravitate towards zero above −2 eV in both V_3As_2 and β-V_4As_3 (Fig. 3).

The bonding analysis of Bouayed et al. (utilizing the Crystal Orbital Overlap Populations [29]) shows that V_3As_2 comprises the ideal electron count, 25 valence-electrons per formula unit, as all bonding interactions are more or less optimized at the Fermi level, E_F, of V_3As_2.

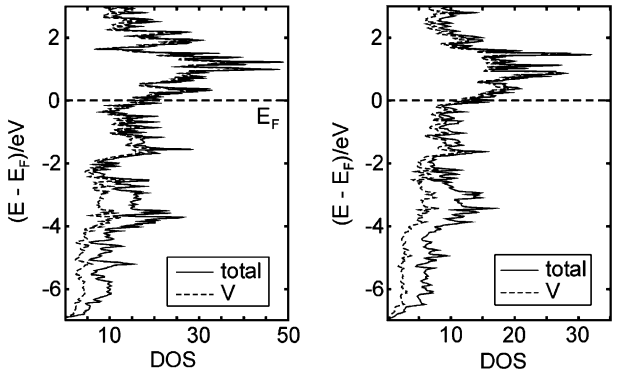

Fig. 2. Densities of states (DOS) of V_3As_2 (left) and β-V_4As_3 (right). The dashed horizontal lines denote the Fermi level E_F, arbitrarily placed at 0 eV.

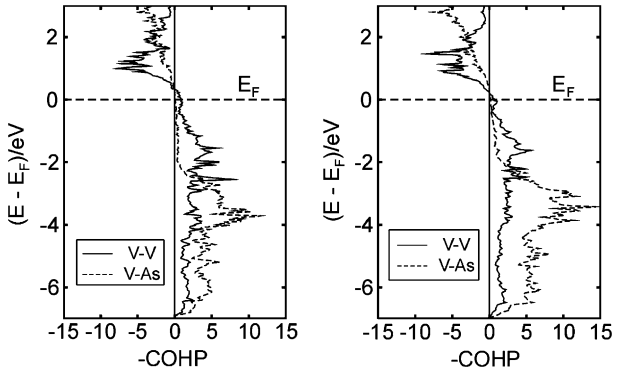

Fig. 3. Cumulated V–V and V–As crystal orbital Hamilton populations (COHP) of V_3As_2 (left) and β-V_4As_3 (right). The dashed horizontal lines denote the Fermi level E_F, arbitrarily placed at 0 eV.

Our COHP calculations support this result for V_3As_2, and point to the same conclusion for β-V_4As_3: while few V–V bonding states remain unfilled at E_F for both V_3As_2 and β-V_4As_3, filling these states would concur with filling antibonding V–As states.

The number of valence-electrons per formula unit of the new ternaries are comparable, with 24 electrons for Ti_2MoAs_2 (V_3As_2: 25) and 33 for Ti_3MoAs_3 (V_4As_3: 35). The computed DOS for our Ti_2MoAs_2 and Ti_3MoAs_3 models (Fig. 4) are very similar to those of V_3As_2 and β-V_4As_3, respectively, revealing that a rigid band model may be assumed. One difference is the lower Fermi level in case of the ternaries, in accord with the lower valence-electron concentrations. Moreover, the Mo states become filled at lower energies than the Ti states, as depicted in the projected DOS, noting the 2:1 and 3:1 ratios of Ti and Mo in Ti_2MoAs_2 and Ti_3MoAs_3.

Last, we consider the ICOHPs of the V–V and V–As interactions, cumulated per V atom, of V_3As_2 and β-V_4As_3. This procedure details which V site participates in the strongest V–V and V–As bonds, and thus helps understanding the preference of Mo for certain sites. Plotting the cumulated ICOHPs of the V arsenides vs. the refined Mo occupancy of the ternaries confirms the two trends discussed above: stronger metal–metal bonding occurs

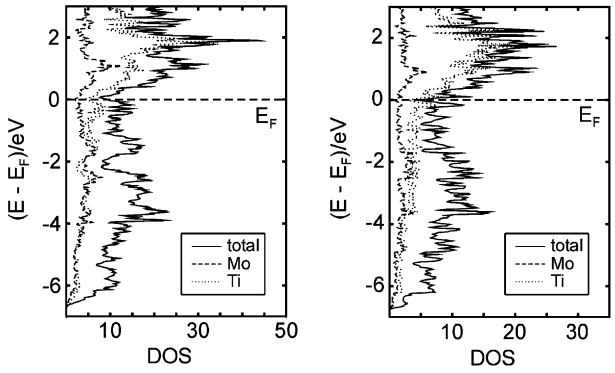

Fig. 4. Densities of states (DOS) of Ti_2MoAs_2 (left) and Ti_3MoAs_3 (right). The dashed horizontal lines denote the Fermi level E_F, arbitrarily placed at 0 eV.

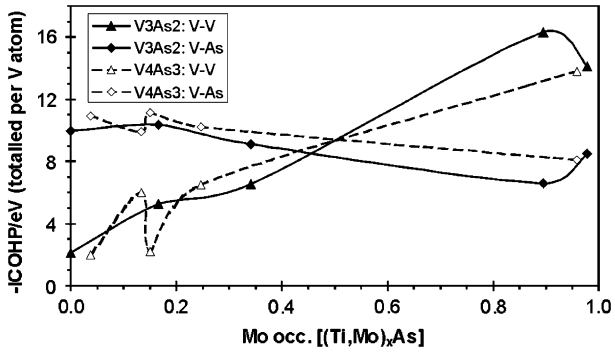

Fig. 5. Cumulated integrated crystal orbital Hamilton population values (ICOHP) per *M* site vs. Mo occupancies.

with higher Mo occupancies, and stronger metal–As bonding with higher Ti occupancies. The apparent exceptions of these trends indicate that the ICOHPs are not the only variables, but important ones as the overall trends are obvious (Fig. 5).

4. Conclusions

Two new ternary metallic arsenides, Ti_2MoAs_2 and Ti_3MoAs_3, were synthesized and characterized. They form structures isotypic with binary V arsenides, namely V_3As_2 and β-V_4As_3, with mixed Ti/Mo occupancies on almost all metal positions. Evidence for the formation of the α-V_4As_3 type was found as well. The preference of titanium for the sites with more M–As and fewer *M–M* bonds is evident. Presumably the α-V_4As_3 structure formed with a starting Ti:Mo ratio of 5:3. The arsenides Ti_2MoAs_2 and Ti_3MoAs_3 are entropy-stabilized high temperature compounds, as they decompose during annealing between 900 and 1200 °C.

This study substantiates the claim that Ti/Mo compounds with Ti:Mo ratios at least between 4:1 and 2:1 may mimic V compounds, since Ti_4MoAs_3 is a substitution variant of $V_{4.95}As_3$, and $Ti_{5.42}Mo_{2.58}Sb_9$ of $V_{7.5}Sb_9$. We are currently investigating Ti/Mo chalcogenides to see whether this concept may be expanded.

Acknowledgments

Financial support from NSERC, CFI, OIT (Ontario Distinguished Researcher Award for HK), the Province of Ontario (Premier's Research Excellence Award for HK) and the Canada Research Chair program (CRC for HK) is appreciated.

References

[1] X. Yao, G. Marking, H.F. Franzen, Ber. Bunsenges. 96 (1992) 1552–1557.
[2] M. Köckerling, H.F. Franzen, Croat. Chem. Acta 68 (1995) 709–719.
[3] X. Yao, H.F. Franzen, J. Solid State Chem. 86 (1990) 88–93.
[4] X. Yao, H.F. Franzen, Z. Anorg. Allg. Chem. 598–599 (1991) 353–362.
[5] X. Yao, H.F. Franzen, J. Am. Chem. Soc. 113 (1991) 1426–1427.
[6] X. Yao, G.J. Miller, H.F. Franzen, J. Alloys Compd. 183 (1992) 7–17.
[7] H. Kleinke, J. Am. Chem. Soc. 122 (2000) 853–860.
[8] H. Kleinke, Inorg. Chem. 40 (2001) 95–100.
[9] H. Kleinke, Inorg. Chem. 38 (1999) 2931–2935.
[10] H. Kleinke, Chem. Commun. (1998) 2219–2220.
[11] H. Kleinke, J. Mater. Chem. 9 (1999) 2703–2708.
[12] J. Cheng, H.F. Franzen, J. Solid State Chem. 121 (1996) 362–371.
[13] C.-S. Lee, E. Dashjav, H. Kleinke, J. Alloys Compd. 338 (2002) 60–68.
[14] A. Assoud, K.M. Kleinke, H. Kleinke, Z. Anorg. Allg. Chem. 631 (2005) 1924–1928.
[15] R. Berger, Acta Chem. Scand. 30A (1976) 363–369.
[16] S. Furuseth, H. Fjellvag, Acta Chem. Scand. 49 (1995) 417–422.
[17] R. Berger, Acta Chem. Scand. 31A (1977) 287–291.
[18] R. Berger, Acta Chem. Scand. 28A (1974) 771–778.
[19] K. Yvon, H. Boller, Monatsh. Chem. 103 (1972) 1643–1650.
[20] The crystal was too small for a structure refinement. The space group (*Cmcm*) and the lattice parameters ($a = 3.493(7)$ Å, $b = 14.12(3)$ Å, $c = 18.61(4)$ Å) point towards the formation of the α-V_4As_3 type (*Cmcm*, $a = 3.42$ Å, $b = 13.73$ Å, $c = 18.12$ Å).
[21] SAINT, Version 4 ed., Siemens Analytical X-ray Instruments Inc., Madison, WI, 1995.
[22] G.M. Sheldrick, SHELXTL, Version 5.12 ed., Siemens Analytical X-ray Systems, Madison, WI, 1995.
[23] O.K. Andersen, Phys. Rev. B 12 (1975) 3060–3083.
[24] H.L. Skriver, The LMTO Method, Springer, Berlin, Germany, 1984.
[25] L. Hedin, B.I. Lundqvist, J. Phys. C 4 (1971) 2064–2083.
[26] P.E. Blöchl, O. Jepsen, O.K. Andersen, Phys. Rev. B 49 (1994) 16223–16233.
[27] R. Dronskowski, P.E. Blöchl, J. Phys. Chem. 97 (1993) 8617–8624.
[28] R.S. Mulliken, J. Chem. Phys. 23 (1955) 2343–2346.
[29] T. Hughbanks, R. Hoffmann, J. Am. Chem. Soc. 105 (1983) 3528–3537.
[30] H.-E. Baurecht, H. Boller, H. Nowotny, Monatsh. Chem. 101 (1970) 1696–1703.
[31] F. Gronvold, A. Kjekshus, Acta Crystallogr. 14 (1961) 930–934.
[32] M.F. Hagedorn, W. Jeitschko, J. Solid State Chem. 119 (1995) 344–348.
[33] L. Pauling, The Nature of the Chemical Bond, third ed, Cornell University Press, Ithaca, NY, 1948.
[34] J.C. Slater, J. Chem. Phys. 41 (1964) 3199–3204.
[35] M. Bouayed, H. Rabaa, A. Le Beuze, S. Deputier, R. Guerin, J.-Y. Saillard, J. Solid State Chem. 154 (2000) 384–389.